Electronic Journal of Structural Engineering

Original Article

Cite this: DOI:10.56748/ejse.25815

Received Date: 01 May 2025
Accepted Date: 25 July 2025

1443-9255
https://ejsei.com/ejse

On the Hysteretic Behavior of Fully Connected and Beam-Connected Flat-Corrugated Steel Shear Walls with Different Corrugation Angles and Orientations

Zhenhua Guan [a*], Linlin Zhang [a]
[a] Anyang Vocational and Technical College, Anyang, Henan, 455000, China
*Corresponding author: FL1989404@163.com

Abstract

Steel Shear Walls (SSWs) have been utilized for years for their significant benefits. In early applications, this system was used without stiffeners, which were subsequently developed and enhanced in multiple ways. A new concept of SSW called Flat-Corrugated Walls (FCWs) has been introduced recently. This research presents a two-layer SSW composed of flat and Corrugated Plates (CPs), in which CPs are used in three directions: horizontal, vertical, and diagonal. Moreover, CPs featuring wave angles of 30°, 45°, and 60° were used. Infill Flat-Corrugated Plates (FCPs) were investigated under two connection conditions: fully connected and connected to beams only. For comparative purposes, Single-Corrugated Steel Shear Walls (SCSSWs) with both fully connected and beam-connected configurations were also examined. This research has shown that the resistance of Fully Connected Flat-Corrugated Walls (FC-FCWs) is higher than that of the corresponding Single-Corrugated Wall (SCW), ranging from 0.4% to 15.6%. In the cases linked to the beam, the resistance of FCWs is at least 0.9% and a maximum of 29.2% higher than the corresponding SCWs. The orientation of the CP in FC-FCWs has a negligible effect on the Hysteresis Curve (HC) and structural parameters, resulting in a stable and reliable performance. While the HC of single-CSSWs is not symmetrical, FCWs have a stable HC, demonstrating the reliability of the system. Increasing the wave angle of the plate has resulted in a greater bearing capacity for flat-CSSWs (FCSSWs). Furthermore, FCSSWs connected to horizontal beams exhibited the lowest resistance among the configurations studied.

Keywords

SSW, Flat-corrugated, Beam-connected, Maximum strength, Damping

1. Introduction

SSWs have gained global popularity in recent decades due to their robust lateral strength, excellent stiffness, outstanding energy absorption capabilities, and flexibility. This system originated in the 1970s (Tan, Gu et al. 2020). Ordinary unstiffened SSWs possess low out-of-plane flexural rigidity (Tong, Guo and Zuo 2018). Thus, they easily experience out-of-plane shear buckling under shear loads, reducing elastic stiffness and energy dissipation capacity. Moreover, SSWs with flat Infill Plates (Ips) experience pinching phenomena in their hysteresis load-displacement curves (Driver, Kulak et al. 1998, Guo, Zhu et al. 2017). In addition to improved SSWs with stiffened Ips (Sabouri-Ghomi and Sajjadi 2012, Alavi and Nateghi 2013, Sigariyazd, Joghataie and Attari 2016, Mu and Yang 2020, Wu, Fan et al. 2023), corrugated SSWs (CSSWs) were introduced as an alternative to flat SSWs (FSSWs) (Dou, Jiang et al. 2016). CSSWs possess more out-of-plane stiffness than Flat Plates (FPs). Consequently, the shear buckling strength of CSSWs surpasses that of FSSWs (Tong, Guo and Zuo 2018).

Some studies have compared the performance of SSWs with FP and CPs. The experimental investigations reported that CSSWs' elastic stiffness and energy absorption are higher than FSSWs (Emami, Mofid and Vafai 2013, Qiu, Zhao et al. 2018). Regarding the placement of the CPs inside the perimeter frame, corrugated shear plates can be installed horizontally, vertically, and diagonally. Since the placement of the corrugations has a significant impact, various studies have been conducted in this regard. To this end, Emami et al. (Emami, Mofid and Vafai 2013), by testing CSSWs in vertical and horizontal directions, reported that their lateral performance is similar. Zheng et al. (Zheng, Wang et al. 2022), by investigating the behavior of CSSWs with horizontal, vertical, and diagonal directions using Abaqus software, concluded that vertical CSSWs have more strength than the other samples. Also, their outcomes displayed that diagonal corrugated walls have an asymmetric HC. Norouzi and Jalaifar (Noruzi and Jalaeefar 2024) found that CSSWs have diagonally higher energy absorption and ultimate strength than others. Qiu et al. (Qiu, Zhao et al. 2018) found that CSSWs have higher lateral strength than horizontal corrugated walls. Zhang et al. (Zhang, Chen et al. 2023) conducted experiments and reported that horizontal CSSWs behave better than vertical CSSWs.

CSSWs have significant weaknesses despite the various advantages. Their first defect is that they have less lateral resistance than FSSWs (Emami, Mofid and Vafai 2013, Qiu, Zhao et al. 2018). In addition, CSSW generally experiences resistance loss after buckling the wavy plate (Broujerdian, Ghamari and Abbaszadeh 2021) and has low post-buckling behavior. This feature contributes to the energy absorption and flexibility of the corrugated wall. Therefore, the researchers thought of improving the behavior of single-CSSWs. One of the designs that yielded satisfactory results was the double-CSSWs introduced by Tong et al. (Tong, Guo and Zuo 2018, Tong, Guo and Pan 2020, Tong, Guo et al. 2020). The system was investigated in other research by various researchers at the laboratory level, all indicating acceptable behavior of the system (Deng, Yang et al. 2022, Ghodratian-Kashan and Maleki 2022, Tong, Wu et al. 2023). In addition to ordinary SSWs, SSWs compounded with flat and corrugated plates were introduced in recent years. In this system, known as flat-corrugated steel shear walls (flat-CSSWs), flat and corrugated plates are used simultaneously. This system can be practiced in various designs. In the first research, Broujerdian et al. (Broujerdian, Ghamari and Abbaszadeh 2021) introduced a combined wall of FP and CPs, in which flat steel plates surrounded a double-corrugated wall. The outcomes showed that this system's behavior was enhanced compared to the single and double CSSWs and FSSWs. Dou et al. (Dou, Xie et al. 2023) tested a flat-walled steel wall with two outer FPs and a sandwich CP. The outcomes displayed that this sample overcomes potential resistance and weakness reduction in single-CSSWs. In another study, LV (Lv 2024) examined the behavior of a flat-CSSW with vertical CPs. Nayel et al. (Nayel, Ghamari and Broujerdian 2022) also examined a semi-supported flat-CSSW. Zand et al. (Zand, Kalatjari and Attari 2024) also tested a three-layer SSW with different configurations. Many forces are applied to SSWs with full connection to boundary members, especially the columns (Ozcelik and Clayton 2017). To overcome this issue, investigators have suggested beam-only-connected SSWs. Though researchers have conducted research in this field (Ghodratian-Kashan and Maleki 2021, Zheng, Zhang et al. 2022, Qiao, Xu et al. 2023), regrettably, minimal investigation has been done on the lateral performance of flat-CSSWs. This study examines the behavior of fully and beam-connected two-layer flat-CSSWs with horizontal, vertical, and diagonal angles under cyclic loading in the Abaqus finite element software (Hibbitt, Karlsson and Sorensen 2002).

2. Method of Study

2.1 Specifications of the Studied Samples

In the current study, at the first step, a trapezoidal single-CSSW was designed at the first stage according to relations presented in Refs

(Sabouri-Ghomi, Ventura and Kharrazi 2005, Farzampour, Mansouri et al. 2018). Based on classical elastic theory, the interactive shear buckling stress of a trapezoidal CP ($\tau^e_{cr.in}$) is achieved in Eq. (1).

$$\left(\frac{1}{\tau^e_{cr.in}}\right)^2 = \left(\frac{1}{\tau^e_{cr.L}}\right)^2 + \left(\frac{1}{\tau^e_{cr.G}}\right)^2 + \left(\frac{1}{\tau_y}\right)^2 \quad (1)$$

Where τ_y displays the shear yield stress. $\tau^e_{cr.L}$ and $\tau^e_{cr.G}$ display the local and global shear buckling stresses, respectively. $\tau^e_{cr.L}$ and $\tau^e_{cr.G}$ are obtained via Eqs. (2) and (3):

$$\tau^e_{cr.L} = \left[5.34 + 4\left(\frac{a}{h}\right)^2\right]\frac{\pi^2 E}{12(1-\mu^2)}\left(\frac{t}{a}\right)^2 \quad (2)$$

$$\tau^e_{cr.G} = \frac{36\varphi E}{[12(1-\mu^2)]^2}\left[\frac{\left(\frac{d}{t}\right)^2+1}{6\gamma}\right]^{0.75}\left(\frac{t}{h}\right)^2 \quad (3)$$

E, ν, t, h, φ and γ are the elastic modulus, Poisson's ratio, the sum of the CP thickness, panel height, boundary condition factor, and flat sub-panel width, respectively. The flat sub-panel width is determined by Eq. (4):

$$\gamma = \frac{a+b}{a+c} \quad (4)$$

Here, a, b, and c are the parameters of the trapezoidal CP, which are displayed in Fig. 1. In this figure, θ is the corrugation angle.

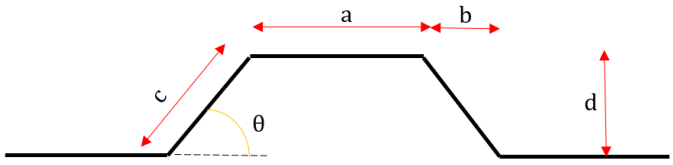

Fig. 1 Parameters of the CP

When $\tau^e_{cr.L}$ and $\tau^e_{cr.G}$ values were obtained via Eqs. (2) and (3), then $\tau^e_{cr.in}$ is obtained via Eq. (1). Hereafter, σty (yield tension field stress) is determined by Eq. (5):

$$\sigma^2_{ty} + (3\tau^e_{cr.in} sin2\theta)\sigma_{ty} + \left(3{\tau^e_{cr.in}}^2 - \sigma^2_y\right) = 0 \quad (5)$$

Next, the boundary components of the perimeter frame, comprising the beam and columns of the CSSW, are fulfilled according to Eqs. (6) and (7):

$$M_{pb} > \frac{\sigma_{ty} t L^2}{8} sin^2(\theta) \quad (6)$$

$$M_{pc} > \frac{\sigma_{ty} t h^2}{8} cos^2(\theta) \quad (7)$$

Where M_{pb} and M_{pc} are the plastic moments of the beam and columns.

Additionally, the column must meet the minimum moment of inertia requirement as indicated in Eq. (8) (Sabelli and Bruneau 2006):

$$I_C > \frac{0.00307 t_w h^4}{L}\mathrm{L} \quad (8)$$

Here, L represents its width, h indicates the panel's height, I_C stands for the column's moment of inertia and t_w signifies the thickness of the web plate. W12x336 and W12x252 cross-sections are utilized for side columns and beams, respectively. Fig. 2 shows the details of the walls under study, while the IP has an 8 mm thickness. The height and width of the perimeter frame are set at 3000 mm.

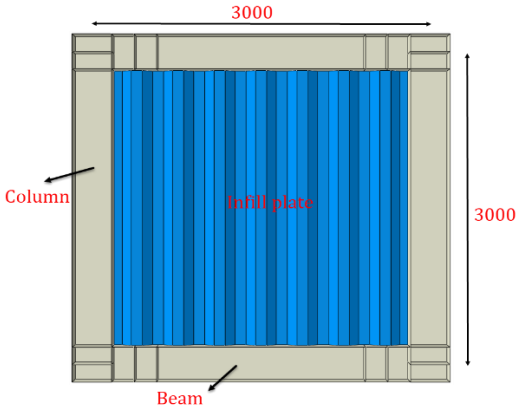

Fig. 2 Geometrical details of the SSW studied in current research

This study considered three orientations for corrugated plates, including horizontal, vertical, and oblique. It is worth noting that for oblique corrugated plates, three angles of inclination of 30°, 45°, and 60° ("α" in Fig. 3) to the horizontal axis were considered. Afterward, flat-corrugated SSWs are investigated in the current paper. A two-layer FCW consists of an FP and a CP, as shown in Fig. 4. Flat and corrugated plates are connected through connecting bolts in the contact areas in a two-layer FCW system. Since the infill plate thickness is considered to be 8 mm, the thickness of each flat and corrugated plate is 4 mm in this new system. As shown in Fig. 5, FCWs are considered with different orientations, including horizontal, vertical, and oblique. In this study, IPs are considered in two different ways. Initially, IPs are completely attached to both beams and columns. In the next step, IPs are connected solely to the beams. Fig. 6 depicts single- and flat-CSSWs connected to beams only.

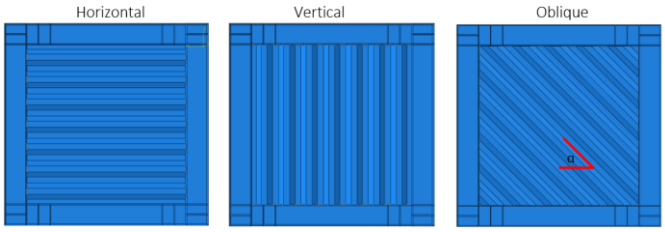

Fig. 3 Single-CSSW with diverse directions

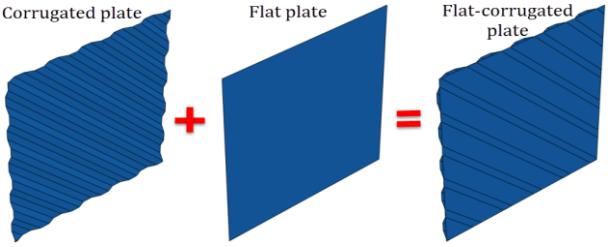

Fig. 4 The FCSSW

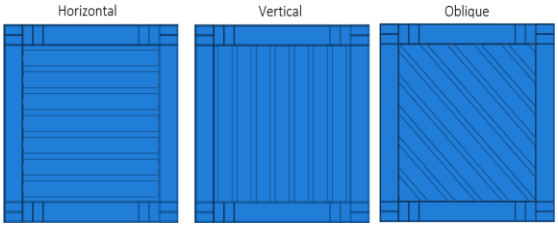

Fig. 5 FCSSW with different directions

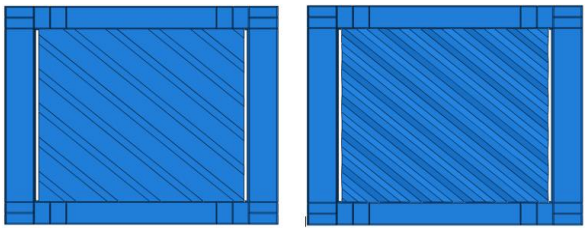

Fig. 6 Beam-connected single- and flat-CSSWs

In this research, three different geometries have been considered for the CPs. Fig. 7 illustrates the geometric details of different CPs. The difference between all the CPs is the wave angle of the plate, which is considered equal to 30, 45, and 60. Other details are the same in all CPs. As stated by Fig. 7, the width of the flat and diagonal sub-plate is 100 mm.

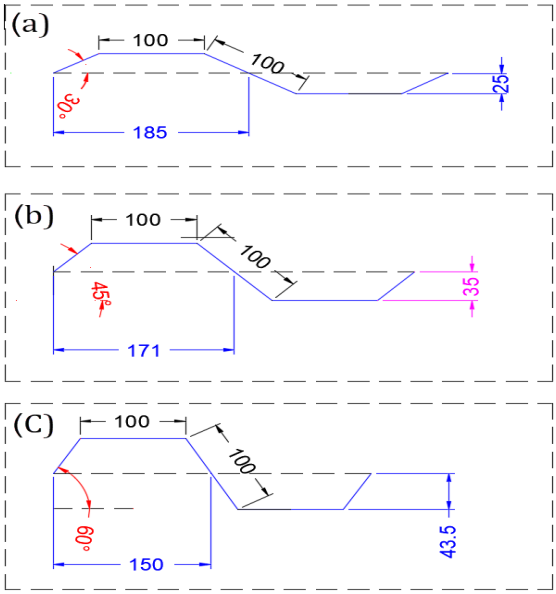

Fig. 7 Geometric details of different CPs a) Wave angle: 30°, b) Wave angle: 45°, c) Wave angle: 60°

S4R shell elements were used in this study to simulate all steel members using Abaqus (2020) software. The Abaqus software utilizes a tie constraint to connect IPs to boundary components. The flat and corrugated plates in the flat-corrugated walls are connected to each other in practice by bolts, providing a unified function. The bolts were not

directly modeled in Abaqus, and instead, bolt locations on the flat and corrugated plates were coupled in the ABAQUS software (Dou, Xie et al. 2023). The bolt spacing was also considered to be a maximum of one-fourth of the plate height and width in the flat-corrugated walls, with vertical and horizontal corrugation orientations, respectively (Tong, Guo and Zuo 2018). In this paper, an elastic-plastic model with a hardening modulus of E_h=E/100 was considered for modeling steel materials in the ABAQUS software. A von Mises yield criterion was adopted to consider the nonlinear behavior of the steel materials (Dou, Xie et al. 2023).

2.2 Boundary Conditions and Lateral Loading

Fig. 8 depicts the boundary conditions of SSWs in the present study. Fixed conditions are considered for the bottom side columns and the bottom beam. Additionally, the panel zone's Out-of-Plane Displacements (OOPDs) were restricted. Following the SAC protocol, the upper beam underwent lateral cyclic loading (Krawinkler 2009). It should be noted that, according to the loading direction, the + sign indicates when the wall is under tension displacements. When the loading direction is -, the CP acts under pressure.

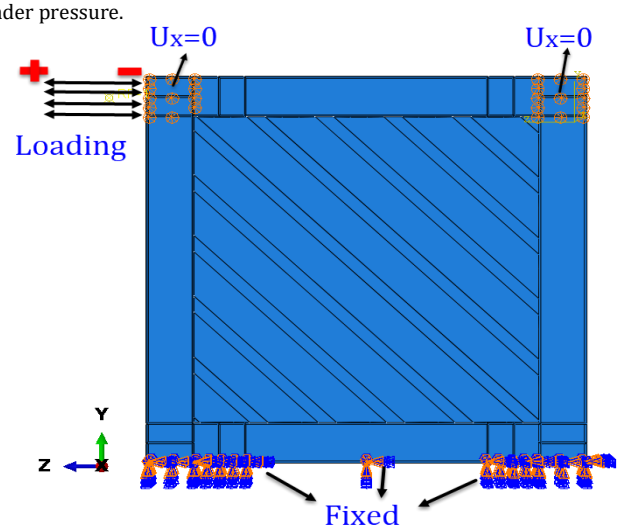

Fig. 8 Boundary conditions of the studied schemes

3. Validation of Numerical Simulations

A flat-CSSW examined by Zhang et al. (Zhang, Chen et al. 2023) was chosen for validation of the numerical model. The geometric details of this specimen are displayed in Fig. 9. An HW150 × 150 × 8 × 7 cross-section was employed for the beam and columns. The column height and beam length are 1530 and 1130 mm, respectively. Fig. 10 demonstrates the details of the CP (Zhang, Chen et al. 2023). As displayed, trapezoidal corrugation was utilized for the IP. The flat sub-plate width is 75 mm. Also, the corrugation depth is 50 mm. Table 1 presents the material properties of the beam web, beam flange, column web, column flange, and infill CP. These values are obtained from the coupon test. Q235 steel served as the material for the steel components.

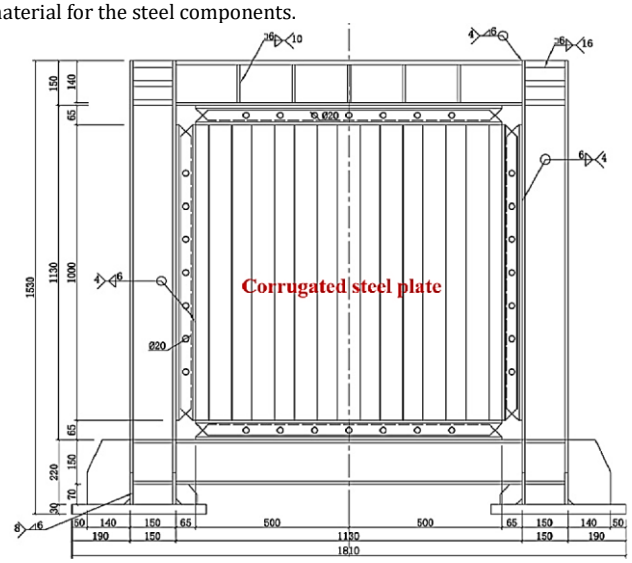

Fig. 9 The details of the CSSW (Zhang, Chen et al. 2023)

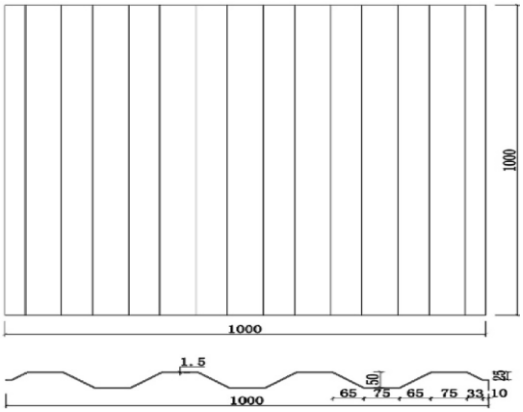

Fig. 10 The details of the CP (Zhang, Chen et al. 2023)

Table 1. Steel material property (Zhang, Chen et al. 2023)

Steel material	Yield strength/MPa	Ultimate tensile strength/ MPa
Beam flange	267	428
Beam web	272	441
column flange	258	432
column web	271	426
Corrugated plate	232	328

Fig. 11 illustrates the test's HC alongside the model generated by Abaqus. The finite element software Abaqus accurately predicts the HC. Also, Fig. 12 compares the test's failure mode with Abaqus modeling. This figure illustrates the software Abaqus' capability to predict the deformed shape of the CSSWs.

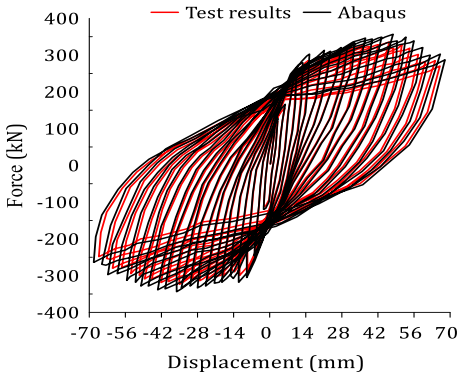

Fig. 11 Analysis of load-displacement graphs for experimental tests and finite element simulations

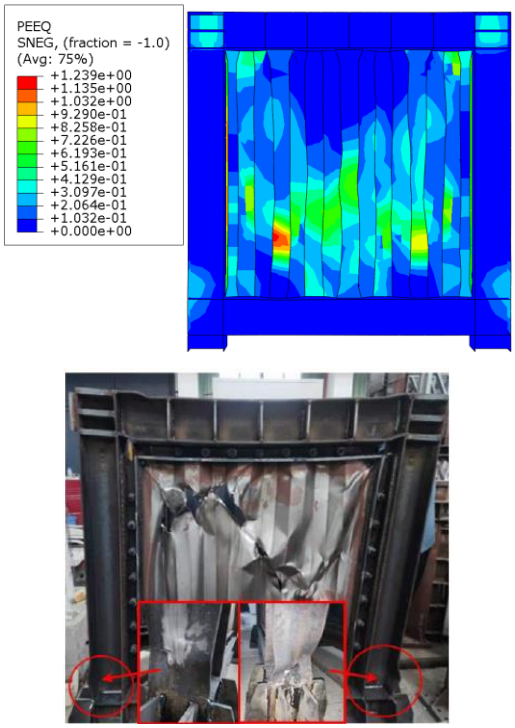

Fig. 12 Analysis of failure mechanisms in testing versus Abaqus simulations

4. Results and Analysis

4.1 Load-Displacement Curves

The load-displacement curves of the samples studied are illustrated in Figs. 13-16. In these figures, the "horizontal" and "vertical" terms refer to FCSSWs and single-CSSWs, respectively, in which corrugated plates are laid horizontally and vertically. In addition, the "inclined" term refers to FCSSWs and single-CSSWs in which corrugated plates are laid obliquely. The numbers in front of the word inclined refer to the corrugation inclination angle of the corrugated plates.

Figs. 13 and 14 show the HCs of fully connected single-corrugated and flat-CSSWs, respectively. According to Fig. 13, the HC of fully connected SCWs is symmetrical in horizontal and vertical directions. Moreover, as the angle of the plate wave increases in these samples, the HCs have become fatter, and the area under the load-displacement diagram has increased. Meanwhile, the HC of SCWs with a vertical direction is asymmetric, and the resistance in the positive loading area is higher than in the compressive area. Fig. 13 also indicates that the growth in the wave angle of the plate has increased the resistance of diagonally corrugated walls.

According to Fig. 14, which shows the HC of FC-FCWs in different directions, it is evident that in these samples, the HC of flat-corrugated samples is symmetrical, similar to that of single-corrugated samples. However, unlike single-corrugated samples with diagonal directions with asymmetric HCs, the HC of FCWs with diagonal CPs is symmetrical. In these examples, the wave angle of the plate affects the load-displacement curve. However, it is not as effective as SCWs.

Fig. 15 presents the HC of the Beam-Connected Flat-Corrugated Wall (BC-FCW). According to this figure, the plate wave angle does not affect the HC of FCWs in the horizontal direction. In BC-FCWs with vertical and diagonal directions, raising the plate's wave angle has increased lateral resistance and the area under the load-displacement diagram. Fig. 16 illustrates the HC of the SCW connected with beams only. This figure shows that the HC of diagonal SCWs is not symmetrical. Also, in these samples with horizontal and diagonal wave directions, the plate wave angle has a small impact on the HC. However, raising the wave angle of the plate has resulted in a greater resistance of the walls in the vertical direction. Maximum Strength

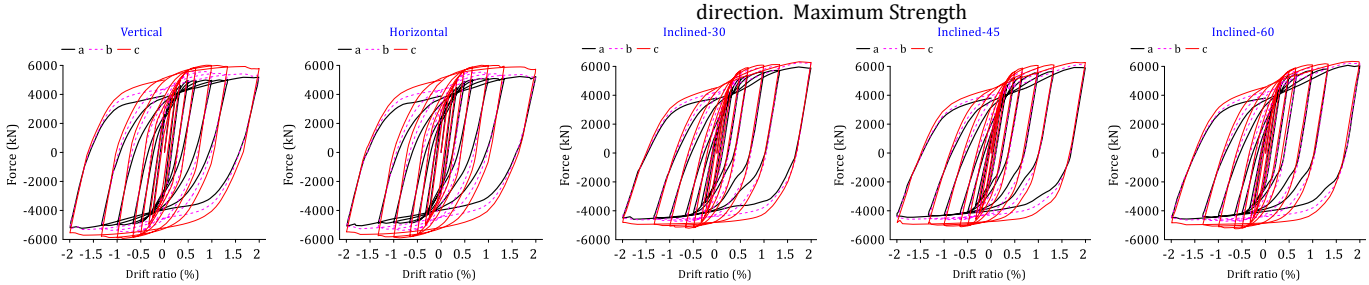

Fig. 13 The hysteresis curve of fully connected single-CSSWs with different corrugation inclinations corrugations and corrugation angles of (a) 30°, (b) 45°, and (c) 60°

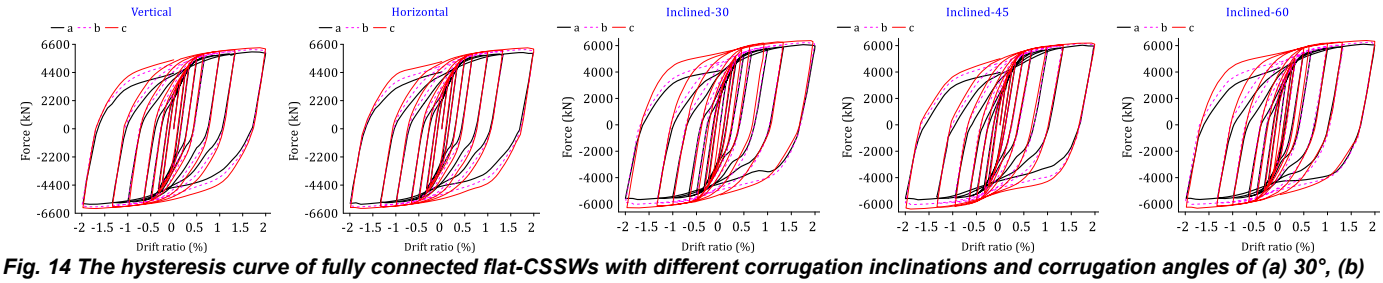

Fig. 14 The hysteresis curve of fully connected flat-CSSWs with different corrugation inclinations and corrugation angles of (a) 30°, (b) 45°, and (c) 60°

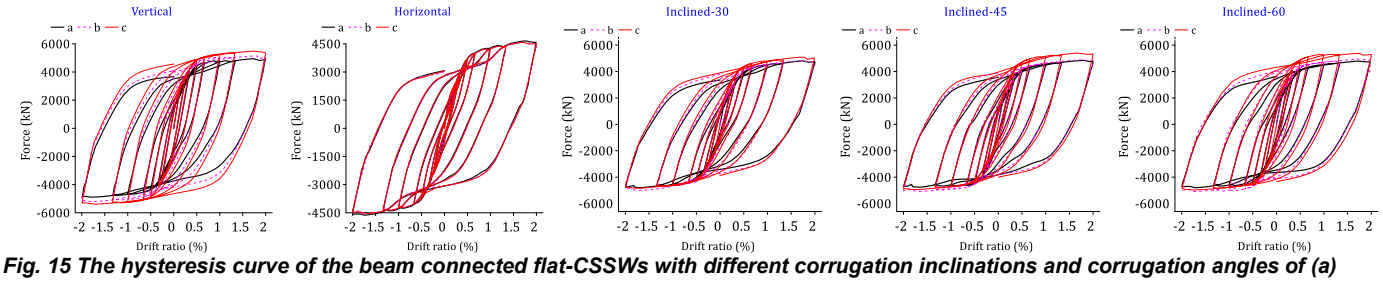

Fig. 15 The hysteresis curve of the beam connected flat-CSSWs with different corrugation inclinations and corrugation angles of (a) 30°, (b) 45°, and (c) 60°

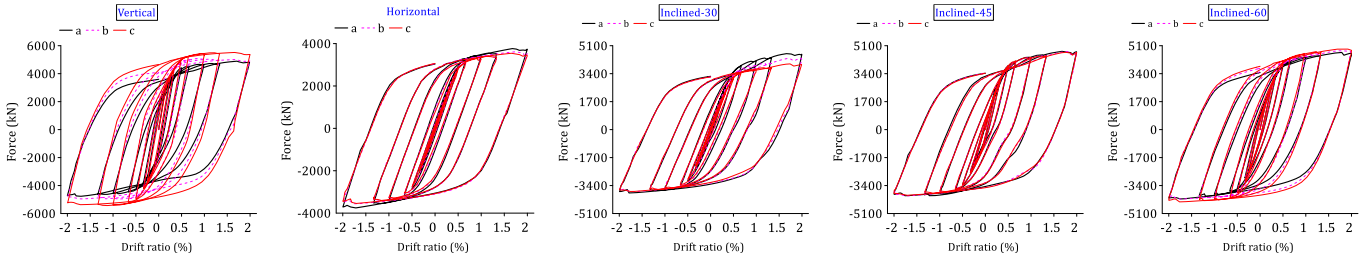

Fig. 16 The hysteresis curve of the beam connected single-CSSWs with different corrugation inclinations and corrugation angles of (a) 30°, (b) 45°, and (c) 60°

The peak resistance comparison for these samples is shown in Fig. 17. In this figure, the numbers in front of the word oblique refer to the corrugation inclination angle of the corrugated plates. The term "Ca" refers to the corrugation angle. The FCWs demonstrate greater strength compared to the single-layer corrugated wall specimens. In walls where IPs are entirely attached to the boundary members, the resistance of FCWs exceeds that of SCWs by at least 0.4% and up to 15.6%. In the beam-connected samples, the resistance of FCWs is higher than that of SCWs, ranging from 0.9% to 29.2%. It is essential to highlight that the most notable distinction between BC-FCWs and SCWs is in the samples with horizontal directions.

Fig. 17 shows that the strength of fully connected flat-CSSWs with different directions increased with the corrugation angle. Also, for a fixed wave angle, the direction of the CP has minimal impact on the maximum resistance of FCWs.

Also, this figure shows that the connection of the IPs in the flat-corrugated system to the beams has decreased the maximum resistance. This resistance reduction ranges from 12.8% to 27.6%. The highest and lowest reductions in resistance occurred in the Horizontal-30 and Oblique-60 samples. Fig. 17 also shows that the corrugated walls with horizontal direction have the lowest resistance among the beam-connected samples. The resistance of the beam-connected corrugated

walls in a vertical direction is higher than that of the corresponding samples in a horizontal direction, with a difference of at least 6.1% and a maximum of 19.6%, depending on the corrugation angle. Additionally, increasing the corrugation angle in FCWs in the horizontal direction has a minimal impact on the peak resistance. However, the increase in the corrugation angle has resulted in increased resistance of the BC-FCWs in vertical and diagonal directions. The findings also show that the inclination angle of the corrugated plates in full-connected FCSSWs has a negligible effect on maximum strength. The maximum difference between these models doesn't exceed 3.1%. The maximum impact of the corrugation inclination angle on the maximum resistance of beam-connected FCSSWs is 6.1%. In contrast, the corrugation inclination angle has a significant effect on the maximum strength of beam-connected single-CSSWs. Increasing the corrugation inclination angle from 30° to 45° and 60° resulted in a maximum resistance increase of 17.6% and 22.4%, respectively. While in fully connected single-CSSWs, increasing the corrugation inclination angle has little impact on the maximum strength (i.e., less than 2.6%).

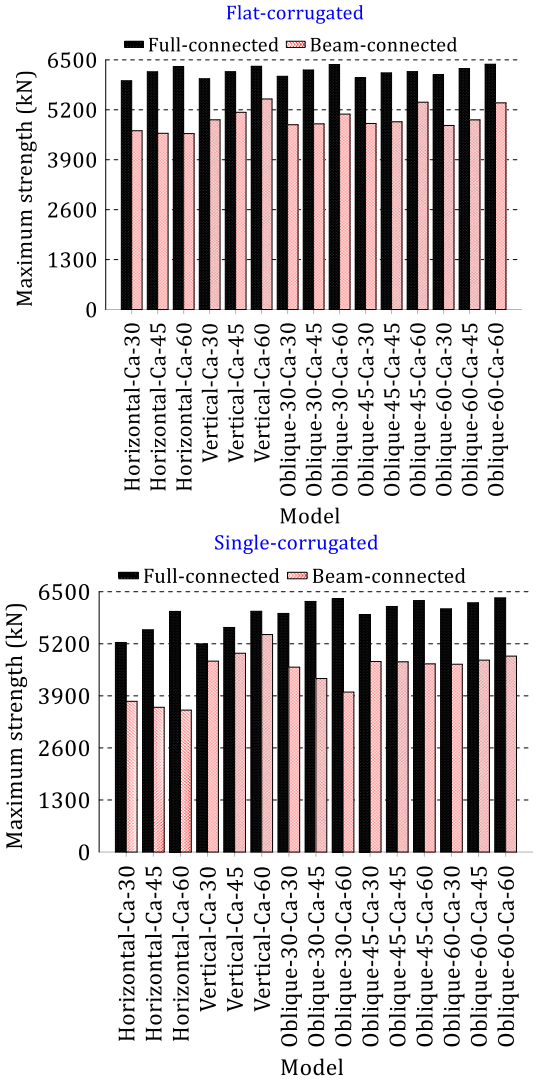

Fig. 17 Comparison of the maximum strength of the studied schemes

4.2 Energy Absorption

Fig. 18 compares the amount of energy absorbed by different samples. As seen, energy absorption in FC-FCWs is greater than in corresponding SCWs. Their difference varies between 1.4% and 13.1%. Additionally, energy absorption in FCWs connected to beams is 1.5% to 21.9% higher than that of the corresponding single-corrugated samples. In addition, energy absorption in FC-FCWs is higher than that of BC-FCWs. Their difference ranges from at least 19.4% to a maximum of 72.9%. Fig. 18 shows that flat-corrugated and single-CSSWs with horizontal corrugation orientations have the lowest energy absorption. Therefore, the use of these types of samples is not recommended. Among the fully connected flat-corrugated and single-corrugated samples, samples with vertical corrugations demonstrate the most significant energy absorption. The results also show that the corrugation inclination angle of the corrugated plate has little effect on the maximum strength of full-connected FCSSWs. In these models, the impact of the corrugation inclination angle on the maximum resistance is ultimately 3.4%. While the maximum effect of the corrugation inclination angle on the maximum strength of the beam-connected FCSSWs is 11.2%. In fully connected single-CSSWs, the corrugation inclination angle has a negligible impact on the maximum strength (i.e., less than 4%). In contrast, the maximum effect of corrugation inclination angle on the maximum strength of beam-connected single-CSSWs is 24.5%. In the beam-connected single-CSSWs, the models with the corrugation inclination angle of 60° have a maximum strength than that of the corresponding models.

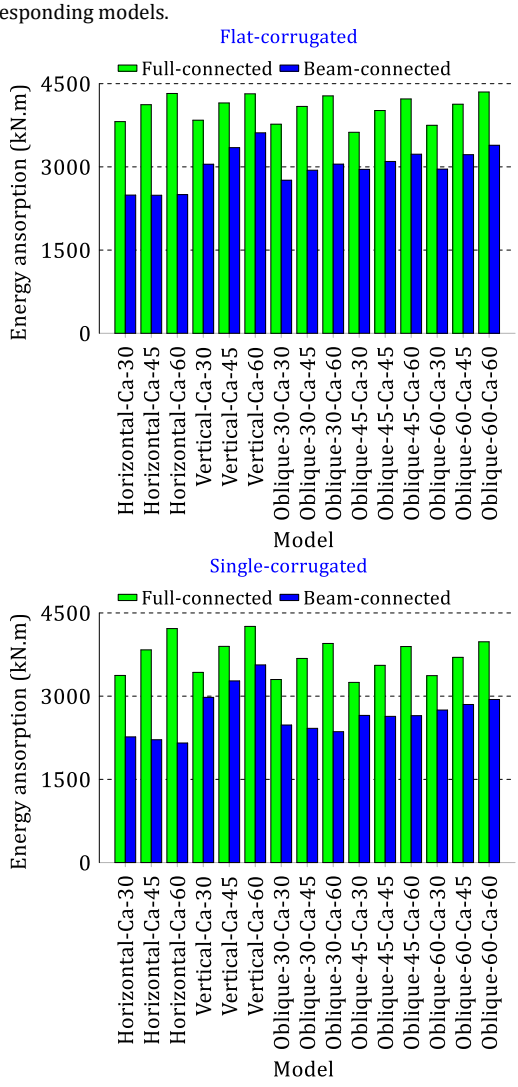

Fig. 18 The comparison of the energy absorption of the examined schemes

4.3 Equivalent Viscous Damping

The equivalent coefficient of viscous damping (ζ_{eq}) is the index presenting the samples' energy dissipation capacity. It is calculated by Eq. (9). Fig. 19 illustrates the parameters of Eq. (9).

$$\zeta_{eq}(\%) = \frac{E_d}{2\pi E_{so}} \times 100 = \frac{S_{(ABC+ACD)}}{2\pi \times S_{(OBE+OFD)}} \times 100 \quad (9)$$

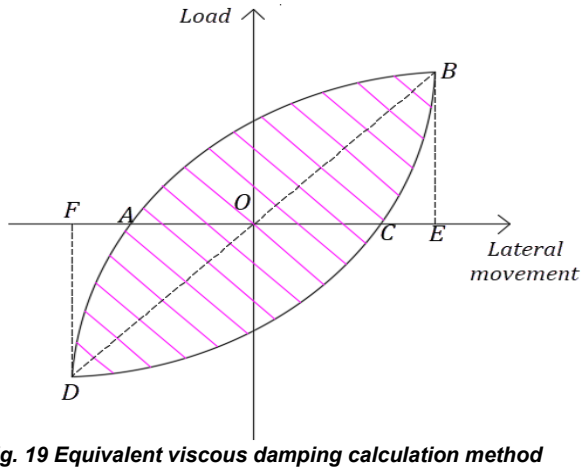

Fig. 19 Equivalent viscous damping calculation method

As shown in Fig. 20, the equivalent viscous resistance in FC-FCWs is slightly higher than that in the corresponding SCWs. Of course, their

difference is less than 4.7%. Additionally, the equivalent viscous damping in FC-FCWs is at least 0.5% and 34.6% higher than that in the corresponding beam-connected samples. Overall, there is minimal variation in the equivalent viscous damping between FCWs and SCWs, regardless of their connections to boundary members.

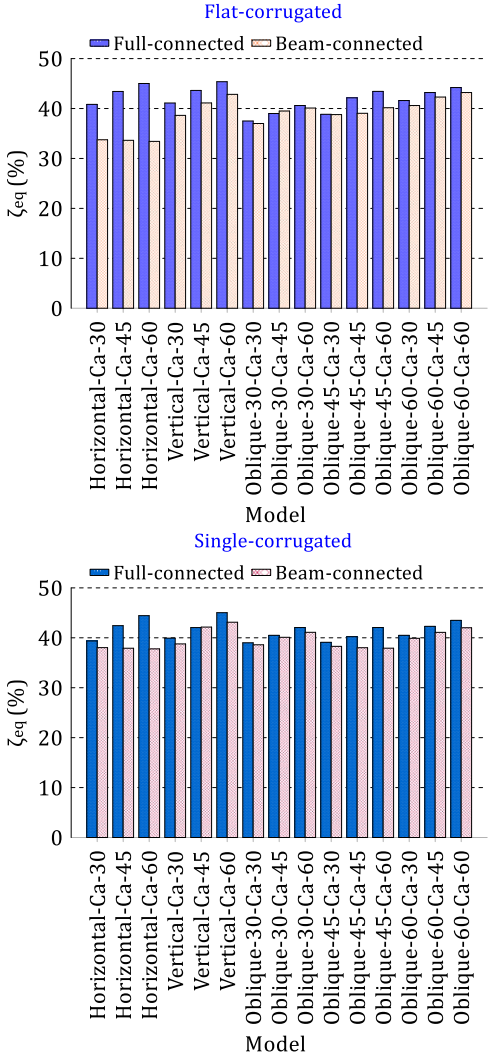

Fig. 20 Comparison of the equivalent viscous damping of the studied schemes

4.4 Deformations

Fig. 21 demonstrates the OOPD distribution of flat-CSSWs at various wave angles for negative and positive loading directions. This figure indicates that the deformation patterns of horizontal and vertical FCWs are similar under negative and positive loading directions. However, the OOPD distribution for FCWs differs from that of a diagonal wave under tension and compression. The comparison of OOPDs of FCWs in horizontal and vertical directions shows that the OOPD of inclined FCWs under the impact of stress is lower than that of the other two samples.

5. Conclusion

This study investigates the lateral behavior of full- and beam-connected SSWs consisting of FCPs with varying corrugation angles and directions under cyclic loading using Abaqus software. The outcomes displayed that the CP's orientation does not significantly affect the hysteresis curve and the structural parameters of fully connected flat-CSSWs, unlike single-CSSWs. Also, the hysteresis curve of the flat-CSSWs with diagonal CPs is symmetrical in contrast to SCWs with diagonal CPs. Among the beam-connected flat-corrugated steel shear walls, the samples with vertical and horizontal CPs have the highest and lowest resistance, respectively. According to the outcomes, energy absorption in FC-FCWs is between 1.4 and 13.1% higher than the corresponding SCWs. Additionally, energy absorption in FCWs connected to beams is 1.5% to 21.9% higher than that of the corresponding single-corrugated samples. In addition, energy absorption in FC-FCWs is higher than that of BC-FCWs. Their difference ranges from at least 19.4% to a maximum of 72.9%. The results also indicate that the corrugation inclination angle in full-connected and beam-connected FCSSWs has a negligible effect on the maximum strength. The maximum difference between these models doesn't exceed 3.1% and 6.1%, respectively. The outcomes also showed that the equivalent viscous damping in beam-connected SSWs is lower than in fully connected corrugated walls. So, the maximum difference in viscous damping of these two samples is 34.6%. The outcomes showed that the viscous damp equivalent to smooth corrugated walls is 4.7% higher than that of fully connected single corrugated walls. The two layer FCSSWs discussed in this study have practical limitations. Since the flat and corrugated plates are connected to each other by bolts, the arrangement of the bolts is a challenge in this field. Connecting flat-corrugated plates to boundary members also has complexities that must be considered in practical designs.

Authorship Contribution Statement

Zhenhua Guan: Writing-Original draft preparation, Conceptualization, Supervision, Project administration.

Linlin Zhang: Methodology, Software

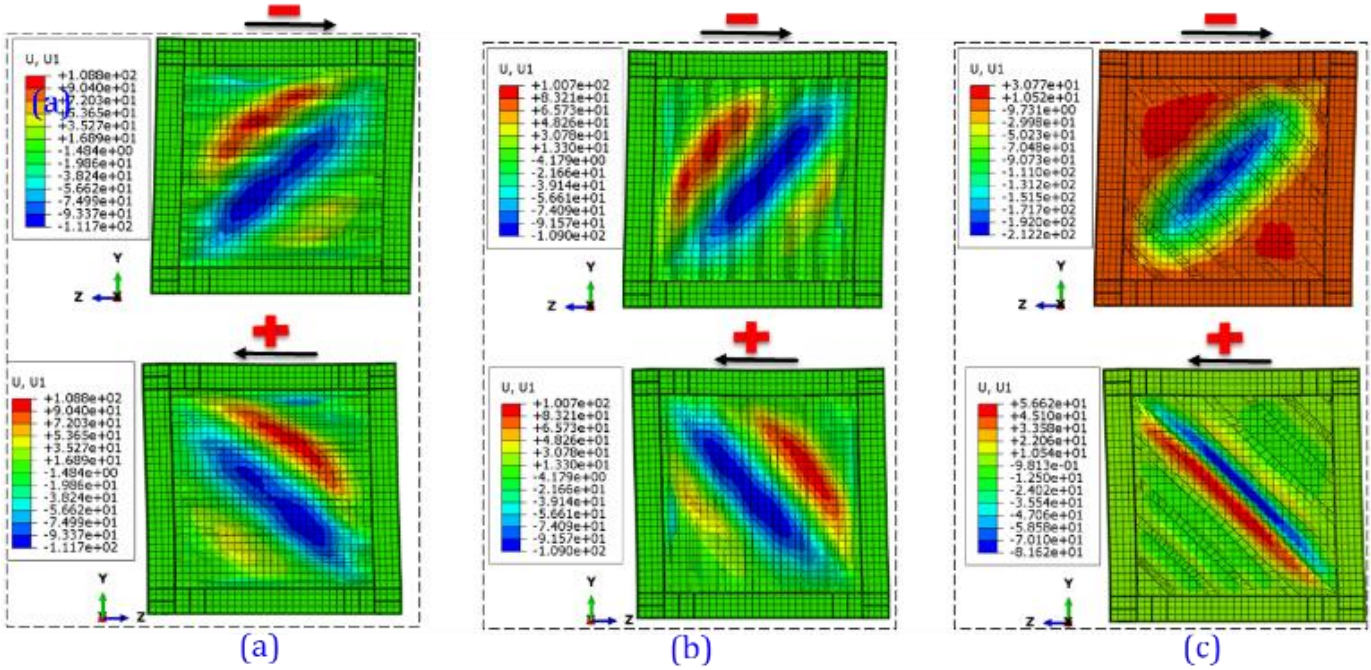

Fig. 21 OOPD distribution of fully connected flat-CSSWs in different directions of loading, (a): Horizontal-30, (b): Vertical-30, (c): Oblique-30

References

Alavi, E. and F. Nateghi (2013). "Experimental study of diagonally stiffened steel plate shear walls." Journal of Structural Engineering 139(11): 1795-1811. https://doi.org/10.1061/(ASCE)ST.1943-541X.0000750

Broujerdian, V., A. Ghamari and A. Abbaszadeh (2021). Introducing an efficient compound section for steel shear wall using flat and corrugated plates. Structures, Elsevier. https://doi.org/10.1016/j.istruc.2021.06.027

Deng, R., J.-D. Yang, Y.-H. Wang, Q.-Q. Li and J.-K. Tan (2022). "Cyclic shear performance of built-up double-corrugated steel plate shear walls: Experiment and simulation." Thin-Walled Structures 181: 110077. https://doi.org/10.1016/j.tws.2022.110077

Dou, C., Z.-Q. Jiang, Y.-L. Pi and Y.-L. Guo (2016). "Elastic shear buckling of sinusoidally corrugated steel plate shear wall." Engineering Structures 121: 136-146. https://doi.org/10.1016/j.engstruct.2016.04.047

Dou, C., C. Xie, Y. Wang and N. Yang (2023). "Cyclic loading test and lateral resistant behavior of flat-corrugated steel plate shear walls." Journal of Building Engineering 66: 105831. https://doi.org/10.1016/j.jobe.2023.105831

Driver, R. G., G. L. Kulak, D. L. Kennedy and A. E. Elwi (1998). "Cyclic test of four-story steel plate shear wall." Journal of Structural Engineering 124(2): 112-120. https://doi.org/10.1061/(ASCE)0733-9445(1998)124:2(112)

Emami, F., M. Mofid and A. Vafai (2013). "Experimental study on cyclic behaviour of trapezoidally corrugated steel shear walls." Engineering Structures 48: 750-762. https://doi.org/10.1016/j.engstruct.2012.11.028

Farzampour, A., I. Mansouri, C.-H. Lee, H.-B. Sim and J. W. Hu (2018). "Analysis and design recommendations for corrugated steel plate shear walls with a reduced beam section." Thin-walled structures 132: 658-666. https://doi.org/10.1016/j.tws.2018.09.026

Ghodratian-Kashan, S. and S. Maleki (2022). "Experimental investigation of double corrugated steel plate shear walls." Journal of Constructional Steel Research 190: 107138. https://doi.org/10.1016/j.jcsr.2022.107138

Ghodratian-Kashan, S. M. and S. Maleki (2021). "Cyclic Performance of Corrugated Steel Plate Shear Walls with Beam-Only-Connected Infill Plates." Advances in Civil Engineering 2021(1): 5542613. https://doi.org/10.1155/2021/5542613

Guo, Y.-L., J.-S. Zhu, P. Zhou and B.-L. Zhu (2017). "A new shuttle-shaped buckling-restrained brace. Theoretical study on buckling behaviour and load resistance." Engineering Structures 147: 223-241. https://doi.org/10.1016/j.engstruct.2017.05.033

Hibbitt, Karlsson and Sorensen (2002). Abaqus/CAE user's manual, Hibbitt, Karlsson & Sorensen, Incorporated.

Krawinkler, H. (2009). Loading histories for cyclic tests in support of performance assessment of structural components. The 3rd international conference on advances in experimental structural engineering, San Francisco.

Lv, P. (2024). "Investigating the behaviour of a steel shear wall consisting of a corrugated and flat plate with fully and semi connections to boundary elements." Multiscale and Multidisciplinary Modeling, Experiments and Design 7(4): 3827-3839. https://doi.org/10.1007/s41939-024-00445-z

Mu, Z. and Y. Yang (2020). "Experimental and numerical study on seismic behaviour of obliquely stiffened steel plate shear walls with openings." Thin-Walled Structures 146: 106457. https://doi.org/10.1016/j.tws.2019.106457

Nayel, I. H., A. Ghamari and V. Broujerdian (2022). "On the behaviour of an innovative four-layer semi-supported steel plate shear wall." Case Studies in Construction Materials 17: e01427. https://doi.org/10.1016/j.cscm.2022.e01427

Noruzi, A. H. and A. Jalaeefar (2024). Effect of corrugated plate arrangements on the performance of steel shear wall frames. Structures, Elsevier. https://doi.org/10.1016/j.istruc.2024.106871

Ozcelik, Y. and P. M. Clayton (2017). "Strip model for steel plate shear walls with beam-connected web plates." Engineering Structures 136: 369-379. https://doi.org/10.1016/j.engstruct.2017.01.051

Qiao, H., H. Xu, X. Zhang, Z. Xing, Y. Chen and E. Tang (2023). "Seismic performance of corrugated steel plate shear walls under various constraint conditions." Thin-Walled Structures 192: 111189. https://doi.org/10.1016/j.tws.2023.111189

Qiu, J., Q. Zhao, C. Yu and Z. Li (2018). "Experimental studies on cyclic behaviour of corrugated steel plate shear walls." Journal of Structural Engineering 144(11): 04018200. https://doi.org/10.1061/(ASCE)ST.1943-541X.0002165

Sabelli, R. and M. Bruneau (2006). Steel plate shear walls, American Institute of Steel Construction.

Sabouri-Ghomi, S. and S. R. A. Sajjadi (2012). "Experimental and theoretical studies of steel shear walls with and without stiffeners." Journal of constructional steel research 75: 152-159. https://doi.org/10.1016/j.jcsr.2012.03.018

Sabouri-Ghomi, S., C. E. Ventura and M. H. Kharrazi (2005). "Shear analysis and design of ductile steel plate walls." Journal of Structural Engineering 131(6): 878-889. https://doi.org/10.1061/(ASCE)0733-9445(2005)131:6(878)

Sigariyazd, M. A., A. Joghataie and N. K. Attari (2016). "Analysis and design recommendations for diagonally stiffened steel plate shear walls." Thin-Walled Structures 103: 72-80. https://doi.org/10.1016/j.tws.2016.02.008

Tan, J.-K., C.-W. Gu, M.-N. Su, Y.-H. Wang, K. Wang, Y. Shi, Y.-S. Lan, W. Luo, X.-W. Deng and Y.-T. Bai (2020). "Finite element modelling and design of steel plate shear wall buckling-restrained by hat-section cold-formed steel members." Journal of Constructional Steel Research 174: 106274. https://doi.org/10.1016/j.jcsr.2020.106274

Tong, J.-Z., Y.-L. Guo and W.-H. Pan (2020). "Ultimate shear resistance and post-ultimate behaviour of double-corrugated-plate shear walls." Journal of Constructional Steel Research 165: 105895. https://doi.org/10.1016/j.jcsr.2019.105895

Tong, J.-Z., Y.-L. Guo and J.-Q. Zuo (2018). "Elastic buckling and load-resistant behaviours of double-corrugated-plate shear walls under pure in-plane shear loads." Thin-Walled Structures 130: 593-612. https://doi.org/10.1016/j.tws.2018.06.021

Tong, J.-Z., Y.-L. Guo, J.-Q. Zuo and J.-K. Gao (2020). "Experimental and numerical study on shear resistant behaviour of double-corrugated-plate shear walls." Thin-Walled Structures 147: 106485. https://doi.org/10.1016/j.tws.2019.106485

Tong, J.-Z., R.-M. Wu, Z.-Y. Xu and Y.-L. Guo (2023). "Subassemblage tests on seismic behaviour of double-corrugated-plate shear walls." Engineering Structures 276: 115341. https://doi.org/10.1016/j.engstruct.2022.115341

Wu, Y., S. Fan, Y. Guo, S. Duan and Q. Wu (2023). "Experimental study and numerical simulation on the seismic behaviour of diagonally stiffened stainless steel plate shear walls under low cyclic loading." Thin-Walled Structures 182: 110165. https://doi.org/10.1016/j.tws.2022.110165

Zand, S. M. D., V. Kalatjari and N. K. Attari (2024). "Cyclic Behaviour of New Steel Plate Shear Walls Reinforced with Trapezoidal Corrugated lates." Periodica Polytechnica Civil Engineering 68(1): 337-348. https://doi.org/10.3311/PPci.22020

Zhang, X., Y. Chen, H. Qiao, W. Kong, C. Zhang, J. Pan and W. Zhang (2023). "Investigation on hysteretic performance of assembled H-shaped steel frame-corrugated steel plate shear wall with different corrugated orientation and wavelength." Journal of Building Engineering 77: 107473. https://doi.org/10.1016/j.jobe.2023.107473

Zheng, H., Z. Zhang, L. Jiang, Y. Hu and W. Wang (2022). "Cyclic performance and shear resistance design of asymmetric diagonal stiffened beam-only-connected corrugated steel plate shear walls." Archives of Civil and Mechanical Engineering 22(4): 183. https://doi.org/10.1007/s43452-022-00502-9

Zheng, L., W. Wang, H. Ge, H. Guo, Y. Gao and Y. Han (2022). "Seismic performance of steel corrugated plate structural walls with different corrugation inclinations." Journal of Constructional Steel Research 192: 107248. https://doi.org/10.1016/j.jcsr.2022.107248

Disclaimer